
Towards Real World Debiasing: A Fine-grained Analysis On Spurious Correlation

Zhibo Wang^{1,2} Peng Kuang^{2,*} Zhixuan Chu^{1,2} Jingyi Wang³ Kui Ren^{1,2}

¹The State Key Laboratory of Blockchain and Data Security, Zhejiang University

²School of Cyber Science and Technology, Zhejiang University

³School of Control Science and Engineering, Zhejiang University

{zhibowang, pengkuang, zhixuanchu, wangjyee, kuiren}@zju.edu.cn

Abstract

Spurious correlations in training data significantly hinder the generalization capability of machine learning models when faced with distribution shifts in real-world scenarios. To tackle the problem, numerous debias approaches have been proposed and benchmarked on datasets intentionally designed with severe biases. However, it remains to be asked: 1. *Do existing benchmarks really capture biases in the real world?* 2. *Can existing debias methods handle biases in the real world?* To answer the questions, we revisit biased distributions in existing benchmarks and real-world datasets, and propose a fine-grained framework for analyzing dataset bias by disentangling it into the magnitude and prevalence of bias. We observe and theoretically demonstrate that existing benchmarks poorly represent real-world biases. We further introduce two novel biased distributions to bridge this gap, forming a nuanced evaluation framework for real-world debiasing. Building upon these results, we evaluate existing debias methods with our evaluation framework. Results show that existing methods are incapable of handling real-world biases. Through in-depth analysis, we propose a simple yet effective approach that can be easily applied to existing debias methods, named Debias in Destruction (DiD). Empirical results demonstrate the superiority of DiD, improving the performance of existing methods on all types of biases within the proposed evaluation framework.

1 Introduction

With the rapid development of machine learning, machine learning systems are increasingly deployed in high-stakes applications such as autonomous driving [1] and medical diagnosis [2], where incorrect decisions may cause severe consequences. As a result, the robustness to distribution shift is crucial in building trustworthy machine learning systems. One of the major reasons why machine learning models fail to generalize to shifted distributions in the real world [3, 4, 5] is because the existence of spurious correlation in training data [6]. Spurious correlation refers to the phenomenon that two distinct concepts are statistically correlated in the training distribution, yet uncorrelated in the test distribution for there is no causal relationship between them [7, 8]. For example, rock wall background may be correlated with the sport climbing in the training data, but they are not causally related and climbing can be indoors or on ice as well [9, 10, 11]. Furthermore, such spurious correlations within the data tend to be captured during training [12], resulting in a biased model that fails to generalize to shifted distributions. In this work, we refer to spurious correlation and bias in datasets interchangeably.

To tackle the problem, various debias methods [9, 12, 13, 14, 15, 16, 17, 18] have been proposed in recent years. And the effectiveness of the methods is benchmarked with synthetic [12, 16, 19]

*Peng Kuang is the corresponding author.

and semi-synthetic [9, 12, 17] (referred as "real-world dataset" in previous works) datasets that are designed to be severely biased. However, while these benchmarks are indeed biased, they are rough and lack thorough consideration of how data is truly biased in the real world. This raises two questions:

1. *Do existing benchmarks really capture biases in the real world?*
2. *Can existing debias methods handle biases in the real world?*

To answer the first question, we revisit the biased distribution in existing benchmarks and real-world datasets, and propose a fine-grained framework for dataset bias analysis. Inspired by the framework proposed by Wiles et al. [6], which assumes the data is composed of some set of attributes, we further claim that analysis of dataset bias should be conducted on the more fine-grained feature (or value) level rather than attribute level, according to our observation on real-world biases. From the claim, we further propose our fine-grained framework that disentangles dataset bias into the magnitude of bias and the prevalence of bias, where the magnitude of bias generally measures how predictive (or biased) features are on the target task and the prevalence of bias generally measures how many samples in the data contain any biased feature. With our framework, we observe that the magnitude and prevalence of real-world biases are both low, in contrast with high magnitude and high prevalence biases in existing benchmarks. In section 3, we theoretically show that two strong assumptions are implicitly held by existing high bias prevalence benchmarks, which further validates our observation that real-world biases are low in bias prevalence.

To answer the second question, we propose two new biased distributions that better mirror biases in the real world. Together with biased distribution in existing benchmarks, we form a fine-grained evaluation framework for real-world debiasing. We focus on biased-auxiliary-model-based debias methods [9, 12, 15, 17, 18, 20], which is the predominant line of work in debiasing, and evaluate the methods with our evaluation framework. Empirical results show that existing methods fail to handle real-world biases. We further conducted an in-depth analysis of existing biased-auxiliary-model-based methods and found that the effectiveness of existing methods is reliant on the high bias prevalence of existing benchmarks and thus fails to handle real-world datasets with low bias prevalence.

Finally, according to our analysis on the biased distributions and existing debias methods [9, 12, 20], we introduce a simple yet effective enhancement to existing biased-auxiliary-model-based methods. Experiments show that our approach improves existing methods on both high and low bias prevalence datasets. To sum up, this work makes the following contributions:

- **Fine-grained analysis and evaluation framework.** We propose a fine-grained framework for analyzing bias in datasets. Based on the framework we further introduce a systematic evaluation framework for real-world debiasing.
- **Theoretical insight.** We derived the hidden strong assumptions held by existing benchmarks, and testify our observation that real-world biases are low in bias prevalence.
- **Principled approach.** A principled approach is proposed based on our analysis, which can be easily applied to existing biased-auxiliary-model-based methods.
- **Empirical validation.** Empirical results on multiple datasets and distributions not only validate our analysis but also demonstrate the superiority of the proposed approach.

2 A Fine-grained Analysis on Bias in Datasets

In this section, we first revisit the biases in existing debiasing benchmarks and biases in the real world. Then, we propose a new framework for assessing dataset bias. Based on the framework we show how existing benchmarks fail to represent bias in real-world conditions.

2.1 Revisiting spurious correlation in datasets

Bias in existing benchmarks. In the area of spurious correlation debiasing, multiple synthetic [12, 16, 19] and semi-synthetic datasets [9, 12, 17] have been adopted to benchmark the effectiveness of the debias methods. Generally, those synthetic datasets first select a target attribute as the learning objective [16], e.g. object, and another spurious attribute that could potentially cause the learned model to be biased, e.g. background. Then, certain sub-groups jointly defined by the target and

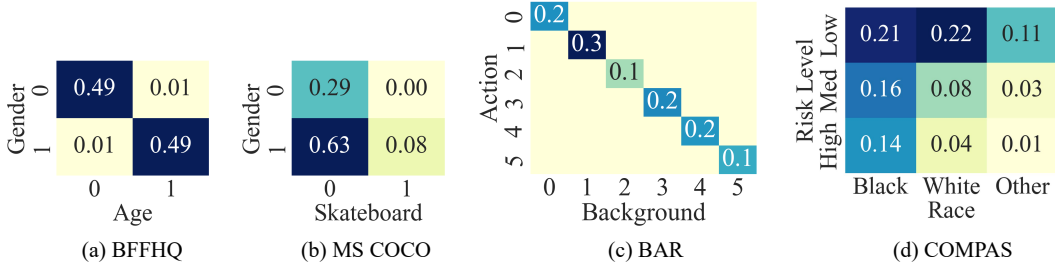


Figure 1: Visualization of the joint distribution for datasets, where the y-axis is the target attribute and the x-axis is the spurious attribute. Figure 1(a) and 1(c) visualise the distribution of existing benchmarks. Figure 1(b) and 1(d) visualize the distribution of real-world datasets. The biased distributions of existing benchmarks and real-world datasets are not alike.

spurious attributes, e.g. water birds with water background, are emphasized, i.e. synthesized or sampled from real-world datasets with much higher probability (usually above 95%) than the others in the biased dataset construction process, causing the corresponding spurious feature and target feature to be spuriously correlated, e.g. water background correlated with water bird [16]. Specifically, one such dominating subgroup is selected for every possible value of the spurious attribute, forming a "diagonal distribution", as shown in Figure 1(a) and 1(c). However, it is critical to examine whether this pattern truly aligns with the complexities of real-world biases.

Bias in the real world. We further investigated biases from the real world. COCO [21] dataset is a large-scale dataset collected from the internet and widely used in various vision tasks. COCO has been found to contain gender bias in web corpora [22], one of which is the spurious correlation between males and skateboards. The joint distribution of gender and Skateboard in COCO is plotted in Figure 1(b). COMPAS [23] dataset consists of the results of a commercial algorithm called COMPAS, used to assess a convicted criminal’s likelihood of reoffending. COMPAS dataset is widely known for its bias against African Americans and is widely used in the research of machine learning fairness [24, 25, 26, 27]. The joint distribution of Race and Risk Level in the COMPAS dataset is plotted in Figure 1(d). Note that although COMPAS is a tabular dataset, it genuinely reflects the biased distribution in the real world. It is quite obvious that the distribution of biases in existing benchmarks and real-world datasets diverges. *More visualizations are shown in Appendix A.* In the following subsection, we will further discuss how to measure their differences.

2.2 Previous measures of spurious correlation

We first revisit measures of spurious correlation in previous works, then point out their insufficiency.

Background. We assume a joint distribution of attributes y^1, y^2, \dots, y^K with $y^k \in A^k$ where A^k is a finite set. One of these K attributes is the target of learning, denoted as y^t , and a spurious attribute y^s with $t \neq s$. The definition of spurious correlation or the measure of bias magnitude is rather vague or flawed in previous works. We summarize the measures in previous works into three categories.

Target attribute conditioned probability. Previous works [19, 28] measure spurious correlation according to the probability of a biased feature a_s within the correlated class a_t : $Corr_{tcp} = P(y^s = a_s | y^t = a_t)$. A higher value of the measure indicates a strong correlation.

Spurious attribute conditioned probability. Some [9, 22, 29, 30] measure spurious correlation according to the probability of the correlated class a_s within samples with biased feature a_t : $Corr_{scp} = P(y^t = a_t | y^s = a_s)$. A higher value of the measure indicates a strong correlation.

Spurious attribute conditioned entropy. Nam et al. [12] defined an entropy-based measure of bias. They use conditional entropy to measure how skewed the conditioned distribution is: $Corr_{sce} = H(y^t | y^s)$, where H is entropy. Values close to 0 indicate a strong correlation. This is an attribute-level measure, yet it is based on information theory.

We then point out the following requirements a proper measure of spurious correlation should satisfy.

Spurious correlation should be measured at the feature level. As shown in Figure 1(a) and 1(c), the predictivity of every value in the spurious attribute is similar in existing benchmarks. However, this is not the case for real-world datasets, where it is clear that the predictivity of values in the spurious attribute varies greatly, as shown in Figure 1(b) and 1(d). Therefore, to deal with real-world biases, analysis of bias should be conducted on a more fine-grained value level, i.e. feature level, rather than attribute level in previous works [12]. Note that though $Corr_{tcp}$ and $Corr_{scp}$ are defined at the feature level, it is assumed by previous works [9, 19, 30] that it is consistent cross features in spurious attribute during benchmark construction, i.e. viewed as an attribute level measure.

The spurious attribute rather than the target attribute should be given as a condition. It is well recognized that the spurious attribute should be easier than the target attribute for the model to learn [12, 30]. Thus the spurious attribute should be more available to the model when learning its decision rules [30] and given as a condition when we define spurious correlation.

The marginal distribution of the target attribute should be accounted for. In $Corr_{tcp}$ and $Corr_{scp}$ measure of spurious correlation, the marginal distribution of the target attribute is not taken into account. This is inaccurate for even if the spurious and the target attribute are statistically independent, the value of $Corr_{tcp}$ and $Corr_{scp}$ could be high if the marginal distribution of spurious and target attribute is highly skewed, e.g. long-tail distributed [31, 32].

Diverge rather than predictivity should be used. While $Corr_{sce}$ satisfies the above requirements, it measures the entropy difference between the conditional and marginal distribution of the target attribute, i.e. the predictivity difference. This is still inaccurate for when the entropy of the distributions is the same, the conditional distribution could still be highly diverged from the marginal distribution, thus highly correlated with the spurious attribute. However, using divergence of the distributions accurately measures how the given condition affects the distribution shift of the target attribute.

2.3 The proposed analysis framework

Given the above requirements that need to be satisfied when measuring spurious correlations, we first propose the following feature-level measure, i.e. bias magnitude.

Bias Magnitude: spurious attribute conditioned divergence. We propose a feature-level measure of spurious correlation that measures the KL divergence between the conditional and marginal distribution of the target attribute:

$$\rho_a^* = Corr_{scd} = KL(P(y^t), P(y^t|y^s = a)) \quad (1)$$

where a is the biased feature (or value) in the spurious attribute. The proposed measure satisfies all the requirements above. The above measure only describes the bias of a given feature in the dataset, i.e. feature-level bias. To further describe the bias level of a dataset, i.e. dataset or attribute level bias, we further define the prevalence of bias.

Bias Prevalence. Consider a set of biased features whose magnitude of the bias is above a certain threshold θ , i.e. $B = \{a|\rho_a^* > \theta\}$. We define the dataset-level bias by taking not only the number but also the prevalence of the biased features:

$$Prv = \sum_{a \in B} P(y^s = a) \quad (2)$$

Here, we further claim and define the existence of Bias-Neutral (BN) samples, referring to samples that do not hold any biased feature defined in B . Bias-Neutral sample is a complement to the previous categorization of samples into Bias-Align (BA) and Bias-Conflict (BC) samples, which is only accurate when all samples in the dataset contain a certain biased feature, assumed by existing synthetic benchmarks [9, 12, 16, 17]. We elaborate on the categorization of samples in Appendix D.

2.4 Observation on real-world biases

Given the dataset assessing framework proposed above, we are now able to analyze how are dataset biases in existing benchmarks different from that in the real world.

The magnitude of biases in real-world datasets is low. As shown in Figure 2(a), the magnitude of biases in real-world datasets is significantly lower than that in existing benchmarks. It is surprising to see how low the magnitude of biases in the COMPAS dataset is, yet still captured by models [26].

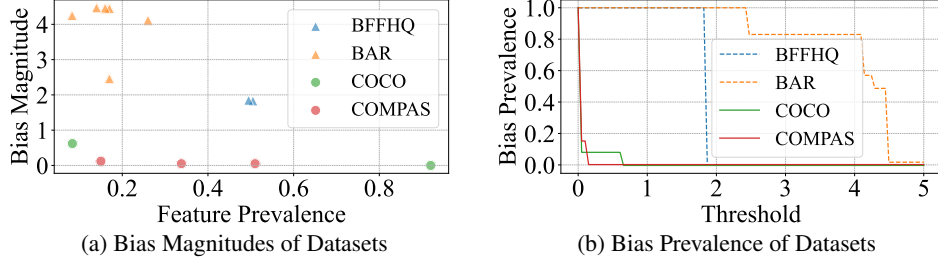


Figure 2: Analysis of datasets bias in existing benchmarks and real-world datasets with the proposed framework. The bias magnitude and prevalence of real-world datasets are significantly smaller than that of existing benchmarks.

The prevalence of bias in real-world datasets is low. As shown in Figure 2(b), the bias prevalence of real-world datasets is also lower than that in existing benchmarks across all thresholds. Considering the bias magnitude of real-world datasets is generally low, it seems fair to set the threshold sufficiently low when calculating the bias prevalence of existing datasets. However, even if we set the threshold to 0.1, the bias prevalence of COCO [21] and COMPAS [23] dataset, i.e. 0.08 and 0.15 respectively, are still significantly lower than that of the existing benchmarks, i.e. 1. *In section 3, we further theoretically show that the above observation is not a mere exception but a manifestation of underlying principles with broader implications.*

3 Theoretical Analysis

In this section, we theoretically show that the high bias prevalence (HP) distribution requires two strong assumptions implicitly held by existing benchmarks. Furthermore, the invalidity of the assumptions in real-world scenarios results in low bias prevalence (LP) distributions.

Data distribution. Consider a classification task on binary target attribute $y^t \sim \{-1, +1\}$ and a binary spurious attribute $y^s \sim \{-1, +1\}$. Let the marginal distribution of the target and spurious attribute be $p_+^t = P(y^t = +1)$ and $p_+^s = P(y^s = +1)$. Then the joint distribution between y^t and y^s can be defined according to the conditional distribution of y^t given $y^s = +1$, i.e. $\tau_+ = P(y^t = +1|y^s = +1)$. We assume that feature $y^s = +1$ and $y^s = -1$ is correlated $y^t = +1$ and $y^t = -1$ respectively, i.e. $\tau_+ > p_+^t$, in the following analysis.

Definition 1 (Simplified Magnitude of Bias). *For the simplicity of theoretical analysis, we propose a simplified version of bias magnitude defined in section 1. Instead of using KL divergence as the measure of distance, we use total variation distance as a proxy for the sake of simplicity:*

$$\rho_+ = \tau_+ - p_+^t, \quad \rho_- = \tau_- - p_-^t \quad (3)$$

The simplification is consistent for it satisfies all the conditions proposed in section 2.

Definition 2 (Biased Feature). *We consider a feature $y^s = a$ is biased if the ratio of its bias magnitude ρ_a to its theoretical maximum $\rho_a^{max} = 1 - p_a^t$ is above certain threshold $0 \leq \theta \leq 1$:*

$$\phi_a = \frac{\rho_a}{\rho_a^{max}} > \theta$$

Definition 3 (High Bias Prevalence Distribution). *We consider distribution as a high bias prevalence distribution only if both of the features in the spurious attribute are biased, i.e. $\phi_+ > \theta, \phi_- > \theta$.*

Note that the definitions above are adjusted and different from those defined in section 2.3 for the simplicity of the analysis. We then propose the two assumptions implied by high prevalence distributions, whose *proof can be found in Appendix C.*

Proposition 1 (High bias prevalence distribution assumes matched marginal distributions). *Assume feature $y^s = +1$ is biased. The high bias prevalence distribution, i.e. feature $y^s = -1$ is biased as well, implying that the marginal distribution of y^t and y^s is matched, i.e. $p_+^t = p_+^s$. Specifically, as θ approaches to 1, the marginal distribution of y^s approaches to that of y^t , i.e. $\lim_{\theta \rightarrow 1} p_+^s = p_+^t$.*

Proposition 2 (High bias prevalence distribution further assumes uniform marginal distributions even if they are matched). *Given that the marginal distribution of y^s and y^t are matched and not uniform,*

i.e. $p = p_+^s = p_+^t < 0.5$. The bias magnitude of sparse feature, i.e. ρ_+^* , is monotone decreasing at p , with $\lim_{p \rightarrow 0^+} \rho_+^* = -\log(1 - \phi_+)$. The bias magnitude of the dense feature, i.e. ρ_-^* , is monotone increasing at p , with $\lim_{p \rightarrow 0^+} \rho_-^* = 0$.

Remark 1. Proposition 2 reveals the fact that as the distribution of attributes becomes increasingly skewed, i.e. p approaches 0, the magnitude of bias for features diverges, the magnitude of sparse increases while the magnitude of dense bias approaches 0. This results in biased sparse features and unbiased dense features, resulting in LP distributions.

4 Methodology

In this section, we dive into how real-world biases would raise a challenge to existing debias methods. Specifically, we focus on debias with biased-auxiliary-model-based (DBAM) methods, which is the mainstream of work in the area of debiasing, and set up the problem in section 4.1. Then we claim the insufficiency of existing DBAM methods facing real-world biases in section 4.2. Finally, aiming at the insufficiency, we proposed our approach in section 4.3.

4.1 Problem setup

Debiasing with biased auxiliary model. In recent years, DBAM methods have been widely studied [9, 12, 15, 17, 18, 20]. Based on the assumption that the spurious attributes are easier and learned more preferentially than the target attribute, these methods use a variant version of cross entropy(CE) that emphasizes easier samples, i.e. generalized cross entropy(GCE) [33], to train a biased auxiliary model M_b . Utilizing the bias captured by the biased auxiliary model, loss-based sample re-weighting scheme $W(x)$ [12] is applied to train the debiased model M_d :

$$W(x) = \frac{CE(M_b(x), y)}{CE(M_d(x), y) + CE(M_b(x), y)} \quad (4)$$

where (x, y) are samples from the training data and $CE(\cdot, \cdot)$ is the cross entropy loss.

4.2 Reliance of DBAM methods on high bias prevalence

We claim that the bias capture module of existing DBAM methods relies on the high bias magnitude of existing benchmarks, which causes failure in real-world debiasing. It is assumed by existing DBAM methods that the biased model M_b predicts according to the bias within the training data, giving high loss to BC samples and low loss to BA samples [9, 12, 15, 17, 18, 20]. Existing works attribute this loss difference to the fact that spurious attributes are easier [12, 17], i.e. learned more preferentially by models, making BA the *easy sample*. While such a claim is true, we claim that the dominance of BA samples in the HP datasets is another vital causing factor of the loss difference, for *dominant/major samples* are learned more frequently than others, as shown in Figure 3(a).

However, on LP datasets, while BA samples are still easier to learn due to the biased feature, the dominant/major samples in the training data are no longer BA samples, but rather BN samples. This not only results in the loss difference between BA and BC samples decreasing but also causes low loss on BN samples, as shown in Figure 3(a). According to sample weighing scheme 4, such low loss on BN samples further leads to low weights for BN samples when training the debiased model, which is unintended because BN samples carry an abundant amount of knowledge concerning the target attribute without the interference of the spurious features. *The overlooking of BN samples results in server utility degradation when existing DBAM methods are applied to LP datasets.* We further empirically testify our claim in section 5.

4.3 Bias capture with feature destruction

Based on our analysis in section 4.2, we introduce a minor yet effective enhancement to the bias capture module in the existing DBAM framework. We name the refined framework as Debias in Destruction (DiD). As shown in Figure 3(b), the problem with the existing bias capture method comes from the side branch learning on BN samples of the biased auxiliary model, which not only captures the bias but also learns the target feature. This is undesired for this further causes the overlooking of BN samples when training the debiased model, as discussed in section 4.2.

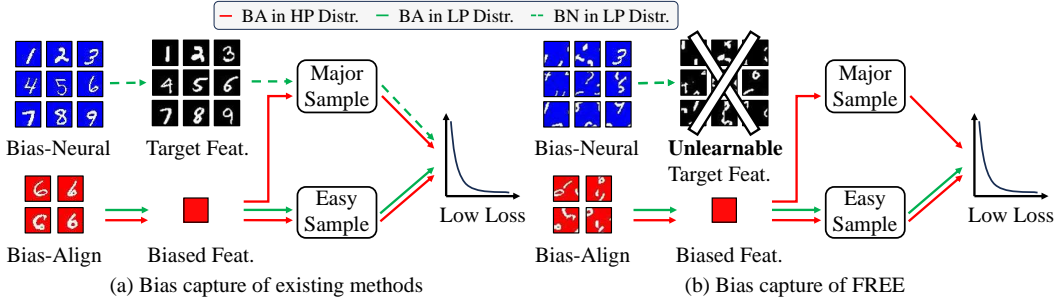


Figure 3: The bias capture process of biased models on LP and HP datasets. Assuming the red background is spuriously correlated with digit 6, and only the major learning of the biased models is illustrated with arrows. DiD eliminates the undesired learning of BN samples on the LP dataset in Figure 3(a) by destroying the target feature, as shown in Figure 3(b).

To prune the side branch learning of the target features, it is intuitive to destroy the target feature and make them unlearnable when training the debiased model, as shown in Figure 3(b). Such action is practical because while the spurious features depend on the distribution of the training data, thus unknown, the target features we intend to learn are usually clear. Specifically, we can achieve this by applying target feature destructive data transformation when training the biased model:

$$Loss_b = GCE(M_b(T_{fd}(x)), y)$$

where $T_{fd}(\cdot)$ is the feature destruction transformation. As an example, in visual recognition tasks, the shape of objects is a basic element of human visual perception [34]. Therefore, the destruction of shape when capturing bias from visual recognition datasets is a feasible approach. Specifically, various approaches can be applied to destroy the shape feature in data [35], e.g. pixel-mixed and patch-mixed image transformation. Here we adopt pixel-mixed image transformation following [35].

5 Experiments

In this section, based on our analysis in section 2, we first propose our fine-grained evaluation framework for real-world debiasing. Then, we design our experiments to answer the following questions: 1) How do existing DBAM methods and DiD perform on real-world biases? 2) Does DiD really emphasize BN samples as we intend? 3) How do debias methods perform on unbiased datasets? 4) How sensitive is DiD to the hyper-parameters? 5) How do the magnitude and prevalence of bias in datasets affect debiasing?

5.1 Fine-grained evaluation framework

As discussed in section 2, biases present in current synthetic benchmarks do not accurately reflect those in the real world. To mirror real-world biases more closely, we introduce two new bias distributions. Together with high magnitude high prevalence (HMHP) biased distribution in existing benchmarks [9, 12, 16, 17], we form our fine-grained evaluation framework for real-world debiasing.

Low Magnitude Low Prevalence (LMLP) Bias. Inspired by the distribution of the COMPAS [23] dataset shown in Figure 2(a), bias in the real world might be low in both magnitude and prevalence.

High Magnitude Low Prevalence (HMLP) Bias. As shown in Figure 2, the COCO [21] dataset may contain features with relatively high bias magnitude, yet low bias prevalence in the dataset due to the sparsity of the biased feature, i.e. low feature prevalence.

Note that datasets with low magnitude high prevalence (LMHP) bias do not exist due to the fact that high bias magnitude is the premise of high bias prevalence. Also, the bias distributions proposed are applicable to existing synthetic and semi-synthetic datasets mentioned in section 2. *More details on how biased distributions are defined and how to synthesize datasets with given distributions can be found in Appendix B.* In this section, we utilize the basic setting of **Colored MNIST** [19] and **Corrupted CIFAR10** [12] for our experiments, details of which can be found in Appendix D.

5.2 Experimental settings

Following previous works [9, 12, 20], we adopt the accuracy of BC samples (**BC**) and the average accuracy on the balanced test set (**Avg**) as the evaluation metrics. We adopt 5 baselines, covering classic and recently proposed DBAM methods. **ERM** directly applies standard training on the biased datasets. **LfF** [12] is the first work to propose the DBAM framework. **DisEnt** [9] disentangles bias and intrinsic features and applies feature augmentation when training the debiased model. **LfF BE** and **DisEnt BE** were recently proposed by Lee et al. [20], and is based on LfF and DisEnt, respectively. These two methods strengthen the bias capture process by applying an ensemble of biased classifiers. Detailed settings can be found in Appendix D.

5.3 Main results

As shown in Table 1, while performing decently on HMHP distributed datasets, existing DBAM methods [9, 12, 20] fail to handle both LMLP and HMLP biases. Generally, for existing DBAM methods, the accuracy of BC samples and the average accuracy on the balanced test set is lower than ERM baseline. This indicates the failure of exiting DBAM methods on the task of debiasing with low bias prevalence datasets, sacrificing utility, i.e. average accuracy, without improving worst group performance, i.e. BC accuracy. Detailed results of existing DBAM methods including the accuracy of all types of samples can be found in Appendix E. We further tested the effectiveness of DiD by combining DiD with existing DBAM methods [9, 12, 20]. As shown in Table 1, after combining DiD, the BC sample accuracy and average accuracy on a balanced test set both improve on existing HMHP benchmarks. On LMLP and HMLP datasets, the superiority of DiD is even more prominent, where BC and average accuracy both improve significantly.

Table 1: The performance of our approach is presented in *absolute accuracy increase* of existing methods. Results show that existing DBAM methods perform poorly on LP distributions, yet our method effectively boosts the performance of existing DBAM methods.

Algorithm	Colored MNIST						Corrupted CIFAR10					
	LMLP		HMLP		HMHP		LMLP		HMLP		HMHP	
	BC	Avg	BC	Avg	BC	Avg	BC	Avg	BC	Avg	BC	Avg
ERM	91.1	91.7	85.2	89.8	48.5	53.4	62.5	64.3	55.9	65.1	29.4	35.4
LfF	68.4	69.7	58.0	63.3	65.6	64.6	55.0	55.4	47.7	54.1	35.3	39.0
+ Ours	+22.6	+21.4	+32.6	+25.8	+1.3	+3.4	+7.0	+7.3	+7.1	+8.9	+1.8	+2.5
LfF BE	83.6	83.5	80.0	82.3	66.9	67.6	52.1	54.0	51.0	54.0	31.5	36.6
+ Ours	+5.7	+6.1	+9.1	+4.9	-0.5	+0.7	+1.1	+0.2	-0.8	+0.1	+1.4	+0.8
DisEnt	73.9	74.9	66.5	72.2	68.3	67.4	55.5	56.1	52.5	54.5	36.0	39.5
+ Ours	+17.2	+16.5	+22.0	+16.8	+0.8	+3.1	+5.4	+5.9	+2.8	+7.1	+3.0	+3.3
DisEnt BE	81.1	81.0	77.6	80.2	67.5	68.5	56.6	57.2	49.1	56.3	34.2	38.6
+ Ours	+8.7	+9.0	+11.7	+5.5	+2.0	+2.5	+4.3	+4.2	+4.9	+5.1	+3.5	+3.2

5.4 Analysis

Emphasis on BN samples. We further validate our method by tracking the weights of samples to see if they match the purpose of our design. Figure 4(a) and 4(b) plots the average weights of all kinds of samples on HMLP distributed Colored MNIST dataset, which shows that the failure of existing methods is indeed caused by the overlooking of BN samples when training the debiased model M_d , as claimed in section 4.2. Figure 4(c) and 4(d) track the sample weight of BN samples when training LfF on HMLP distribution. As we can see, our proposed approach significantly raise the weights of the BN sample, which further demonstrates the effectiveness of our design.

Debias on unbiased datasets. As we do not know how biased or is the training data biased at all in real-world scenarios, it is important to evaluate the performance of debias methods on unbiased training data to ensure that they do not cause severe performance degradation, if not improving the performance. As shown in Table 2, existing DBAM methods perform poorly on unbiased training data, causing severe performance degradation, yet our approach greatly boosts their performances.

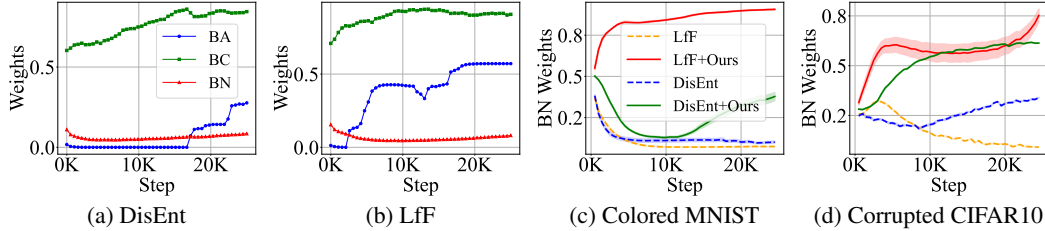


Figure 4: Figure 4(a) and 4(b) support our claim in section 4 that existing DBAM methods tend to overlook BN samples when training on LP distributions. Figure 4(a) and 4(b) show that our approach effectively emphasizes BN samples by raising its weights.

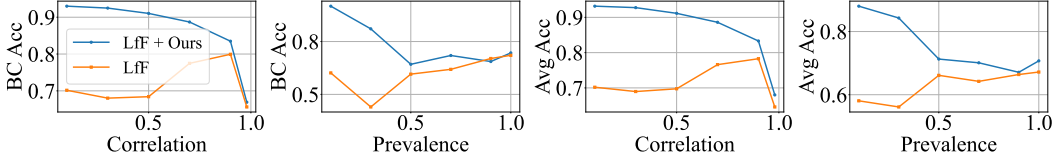


Figure 5: The performance of debias methods under various bias magnitudes and prevalence.

Hyper-parameter sensitivity. We examine three feature destruction methods: pixel-shuffling, patch-shuffling, and center occlusion, to destroy object shapes. We observed that patch-shuffle with patch-size 8 exhibits the best performance on Corrupted CIFAR10 which is of size 32x32.

Effect of bias magnitude and prevalence in debiasing. As shown in Figure 5, we use the correlation $Corr_{scp}$ defined in section 2 as a proxy for the bias magnitude and vary it from low to high. With the increase of the bias magnitude, the performance of LfF first increases as the data become biased, and then decreases as the bias magnitude becomes extremely high, while DiD consistently improves the performance. As shown in 5, we vary the prevalence of bias by controlling the number of biased features, which can also be viewed as an interpolation between HMLP and HMHP distribution. With the increase of the bias prevalence, the performance of LfF generally keeps increasing for its reliance on high prevalence as discussed in section 4, while DiD consistently improves the performance. Those experiments are conducted on Colored MNIST dataset.

Table 2: Existing DBAM methods perform poorly on unbiased training data, while DiD greatly boosts the performance.

Algorithm	Colored MNIST	Corrupted CIFAR10
ERM	94.14 \pm 0.21	67.91 \pm 0.13
LfF	70.19 \pm 1.50	52.04 \pm 2.14
+ Ours	93.18 \pm 0.26	57.29 \pm 0.22
LfF BE	84.14 \pm 0.61	55.64 \pm 0.66
+ Ours	90.02 \pm 0.54	56.28 \pm 0.45
DisEnt	75.24 \pm 3.40	58.50 \pm 0.20
+ Ours	92.24 \pm 0.44	64.58 \pm 0.02
DisEnt BE	80.66 \pm 0.90	58.57 \pm 0.12
+ Ours	89.10 \pm 1.28	62.97 \pm 0.16

Table 3: We experiment with three feature destruction methods with various hyper-parameters on HMLP distributed dataset with LfF.

T_{fd}	param	BC	Avg
N/A	N/A	47.70 \pm 3.58	54.15 \pm 3.02
pixel-shuffle	1	51.44 \pm 1.01	55.43 \pm 0.20
	2	51.07 \pm 0.48	55.29 \pm 0.27
	4	49.41 \pm 0.26	55.40 \pm 0.26
	8	54.81 \pm 0.74	63.06 \pm 0.77
patch-shuffle	8	54.81 \pm 0.74	63.06 \pm 0.77
	16	49.74 \pm 1.10	53.69 \pm 0.31
center-occlusion	8	45.19 \pm 1.41	51.61 \pm 1.31
	16	47.26 \pm 0.54	50.94 \pm 0.59
	24	49.00 \pm 0.80	52.60 \pm 0.55
	32	52.44 \pm 0.87	55.76 \pm 0.16

6 Conclusions and Discussion

In this work, we emphasize the importance of debias within the real world. To tackle real-world biases, we first proposed a fine-grained analysis framework to analyze dataset biases, based on which we further proposed a systematic evaluation framework for benchmarking debias methods under real-world biases. According to our result, we identified the insufficiency of existing methods and proposed a new approach to resolve it. Our experiments demonstrate the effectiveness of our approach. In Appendix G, we further discuss the limitations and future directions of this work.

References

- [1] Joel Janai, Fatma Güney, Aseem Behl, and Andreas Geiger. Computer vision for autonomous vehicles: Problems, datasets and state of the art, 2021.
- [2] Ibrahim Ibrahim and Adnan Abdulazeez. The Role of Machine Learning Algorithms for Diagnosing Diseases. *Journal of Applied Science and Technology Trends*, 2(01):10–19, March 2021. doi: 10.38094/jastt20179.
- [3] Pang Wei Koh, Shiori Sagawa, Henrik Marklund, Sang Michael Xie, Marvin Zhang, Akshay Balsubramani, Weihua Hu, Michihiro Yasunaga, Richard Lanus Phillips, Irena Gao, Tony Lee, Etienne David, Ian Stavness, Wei Guo, Berton Earnshaw, Imran Haque, Sara M Beery, Jure Leskovec, Anshul Kundaje, Emma Pierson, Sergey Levine, Chelsea Finn, and Percy Liang. WILDS: A benchmark of in-the-Wild distribution shifts. In Marina Meila and Tong Zhang, editors, *Proceedings of the 38th International Conference on Machine Learning*, volume 139 of *Proceedings of Machine Learning Research*, pages 5637–5664. PMLR, 2021-07-18/2021-07-24.
- [4] Zhixuan Chu, Ruopeng Li, Stephen Rathbun, and Sheng Li. Continual causal inference with incremental observational data. In *2023 IEEE 39th International Conference on Data Engineering (ICDE)*, pages 3430–3439. IEEE, 2023.
- [5] Siqiao Xue, Yan Wang, Zhixuan Chu, Xiaoming Shi, Caigao Jiang, Hongyan Hao, Gangwei Jiang, Xiaoyun Feng, James Zhang, and Jun Zhou. Prompt-augmented temporal point process for streaming event sequence. *Advances in Neural Information Processing Systems*, 36:18885–18905, 2023.
- [6] Olivia Wiles, Sven Gowal, Florian Stimberg, Sylvestre-Alvise Rebuffi, Ira Ktena, Krishna-murthy Dj Dvijotham, and Ali Taylan Cemgil. A fine-grained analysis on distribution shift. In *International Conference on Learning Representations*, 2022.
- [7] Liuyi Yao, Zhixuan Chu, Sheng Li, Yaliang Li, Jing Gao, and Aidong Zhang. A survey on causal inference. *ACM Transactions on Knowledge Discovery from Data (TKDD)*, 15(5):1–46, 2021.
- [8] Zhixuan Chu and Sheng Li. Causal effect estimation: Recent progress, challenges, and opportunities. *Machine Learning for Causal Inference*, pages 79–100, 2023.
- [9] Jungsoo Lee, Eungyeup Kim, Juyoung Lee, Jihyeon Lee, and Jaegul Choo. Learning debiased representation via disentangled feature augmentation. In M. Ranzato, A. Beygelzimer, Y. Dauphin, P.S. Liang, and J. Wortman Vaughan, editors, *Advances in Neural Information Processing Systems*, volume 34, pages 25123–25133. Curran Associates, Inc., 2021.
- [10] Zhixuan Chu, Stephen L Rathbun, and Sheng Li. Graph infomax adversarial learning for treatment effect estimation with networked observational data. In *Proceedings of the 27th ACM SIGKDD Conference on Knowledge Discovery & Data Mining*, pages 176–184, 2021.
- [11] Zhixuan Chu, Stephen L Rathbun, and Sheng Li. Matching in selective and balanced representation space for treatment effects estimation. In *Proceedings of the 29th ACM International Conference on Information & Knowledge Management*, pages 205–214, 2020.
- [12] Junhyun Nam, Hyuntak Cha, Sungsoo Ahn, Jaeho Lee, and Jinwoo Shin. Learning from failure: De-biasing classifier from biased classifier. In H. Larochelle, M. Ranzato, R. Hadsell, M.F. Balcan, and H. Lin, editors, *Advances in Neural Information Processing Systems*, volume 33, pages 20673–20684. Curran Associates, Inc., 2020.
- [13] Hyojin Bahng, Sanghyuk Chun, Sangdoo Yun, Jaegul Choo, and Seong Joon Oh. Learning de-biased representations with biased representations. In *Proceedings of the 37th International Conference on Machine Learning, ICML’20*. JMLR.org, 2020.
- [14] Eungyeup Kim, Jihyeon Lee, and Jaegul Choo. BiaSwap: Removing dataset bias with bias-tailored swapping augmentation. In *Proceedings of the IEEE/CVF International Conference on Computer Vision (ICCV)*, pages 14992–15001, October 2021.
- [15] Nayeong Kim, SEHYUN HWANG, Sungsoo Ahn, Jaesik Park, and Suha Kwak. Learning debiased classifier with biased committee. In S. Koyejo, S. Mohamed, A. Agarwal, D. Belgrave, K. Cho, and A. Oh, editors, *Advances in Neural Information Processing Systems*, volume 35, pages 18403–18415. Curran Associates, Inc., 2022.

- [16] Evan Z Liu, Behzad Haghgoo, Annie S Chen, Aditi Raghunathan, Pang Wei Koh, Shiori Sagawa, Percy Liang, and Chelsea Finn. Just train twice: Improving group robustness without training group information. In Marina Meila and Tong Zhang, editors, *Proceedings of the 38th International Conference on Machine Learning*, volume 139 of *Proceedings of Machine Learning Research*, pages 6781–6792. PMLR, 2021-07-18/2021-07-24.
- [17] Jongin Lim, Youngdong Kim, Byungjai Kim, Chanho Ahn, Jinwoo Shin, Eunho Yang, and Seungju Han. BiasAdv: Bias-Adversarial Augmentation for Model Debiasing. In *Proceedings of the IEEE/CVF Conference on Computer Vision and Pattern Recognition (CVPR)*, pages 3832–3841, June 2023.
- [18] Bowen Zhao, Chen Chen, Qian-Wei Wang, Anfeng He, and Shu-Tao Xia. Combating Unknown Bias with Effective Bias-Conflicting Scoring and Gradient Alignment. *Proceedings of the AAAI Conference on Artificial Intelligence*, 37(3):3561–3569, June 2023. doi: 10.1609/aaai.v37i3.25466.
- [19] Charan Reddy, Deepak Sharma, Soroush Mehri, Adriana Romero Soriano, Samira Shabani, and Sina Honari. Benchmarking Bias Mitigation Algorithms in Representation Learning through Fairness Metrics. In J. Vanschoren and S. Yeung, editors, *Proceedings of the Neural Information Processing Systems Track on Datasets and Benchmarks*, volume 1, 2021.
- [20] Jungsoo Lee, Jeonghoon Park, Daeyoung Kim, Juyoung Lee, Edward Choi, and Jaegul Choo. Revisiting the Importance of Amplifying Bias for Debiasing. *Proceedings of the AAAI Conference on Artificial Intelligence*, 37(12):14974–14981, June 2023. ISSN 2374-3468, 2159-5399. doi: 10.1609/aaai.v37i12.26748.
- [21] Tsung-Yi Lin, Michael Maire, Serge Belongie, Lubomir Bourdev, Ross Girshick, James Hays, Pietro Perona, Deva Ramanan, C. Lawrence Zitnick, and Piotr Dollár. Microsoft COCO: Common objects in context, 2015.
- [22] Ruixiang Tang, Mengnan Du, Yuening Li, Zirui Liu, Na Zou, and Xia Hu. Mitigating gender bias in captioning systems. In *Proceedings of the Web Conference 2021, WWW '21*, pages 633–645, New York, NY, USA, 2021. Association for Computing Machinery. ISBN 978-1-4503-8312-7. doi: 10.1145/3442381.3449950.
- [23] Mattu, Jeff Larson, Lauren Kirchner, Surya, and Julia Angwin. Machine Bias. *ProPublica*, 2016.
- [24] Naman Goel, Mohammad Yaghini, and Boi Faltings. Non-Discriminatory Machine Learning Through Convex Fairness Criteria. *Proceedings of the AAAI Conference on Artificial Intelligence*, 32(1), April 2018. doi: 10.1609/aaai.v32i1.11662.
- [25] Max Hort, Jie M. Zhang, Federica Sarro, and Mark Harman. Fairea: A Model Behaviour Mutation Approach to Benchmarking Bias Mitigation Methods. In *Proceedings of the 29th ACM Joint Meeting on European Software Engineering Conference and Symposium on the Foundations of Software Engineering, ESEC/FSE 2021*, pages 994–1006, New York, NY, USA, 2021. Association for Computing Machinery. ISBN 978-1-4503-8562-6. doi: 10.1145/3468264.3468565.
- [26] Peizhao Li and Hongfu Liu. Achieving Fairness at No Utility Cost via Data Reweighting with Influence. In Kamalika Chaudhuri, Stefanie Jegelka, Le Song, Csaba Szepesvari, Gang Niu, and Sivan Sabato, editors, *Proceedings of the 39th International Conference on Machine Learning*, volume 162 of *Proceedings of Machine Learning Research*, pages 12917–12930. PMLR, July 2022.
- [27] Dongliang Guo, Zhixuan Chu, and Sheng Li. Fair attribute completion on graph with missing attributes. *arXiv preprint arXiv:2302.12977*, 2023.
- [28] Angelina Wang and Olga Russakovsky. Overwriting pretrained bias with finetuning data. In *Proceedings of the IEEE/CVF International Conference on Computer Vision (ICCV)*, pages 3957–3968, October 2023.
- [29] Sriram Yenamandra, Pratik Ramesh, Viraj Prabhu, and Judy Hoffman. FACTS: First amplify correlations and then slice to discover bias. In *Proceedings of the IEEE/CVF International Conference on Computer Vision (ICCV)*, pages 4794–4804, October 2023.
- [30] Katherine Hermann, Hossein Mobahi, Thomas FEL, and Michael Curtis Mozer. On the foundations of shortcut learning. In *The Twelfth International Conference on Learning Representations*, 2024.

- [31] Songyang Zhang, Zeming Li, Shipeng Yan, Xuming He, and Jian Sun. Distribution alignment: A unified framework for long-tail visual recognition. In *Proceedings of the IEEE/CVF Conference on Computer Vision and Pattern Recognition*, pages 2361–2370, 2021.
- [32] Yifan Zhang, Bingyi Kang, Bryan Hooi, Shuicheng Yan, and Jiashi Feng. Deep long-tailed learning: A survey. *IEEE Transactions on Pattern Analysis and Machine Intelligence*, 2023.
- [33] Zhilu Zhang and Mert R. Sabuncu. Generalized cross entropy loss for training deep neural networks with noisy labels. In *Proceedings of the 32nd International Conference on Neural Information Processing Systems, NIPS’18*, pages 8792–8802, Red Hook, NY, USA, 2018. Curran Associates Inc.
- [34] Robert Geirhos, Patricia Rubisch, Claudio Michaelis, Matthias Bethge, Felix A. Wichmann, and Wieland Brendel. ImageNet-trained CNNs are biased towards texture; increasing shape bias improves accuracy and robustness. In *International Conference on Learning Representations*, 2019.
- [35] Jonghyun Lee, Dahuin Jung, Saehyung Lee, Junsung Park, Juhyeon Shin, Uiwon Hwang, and Sungroh Yoon. Entropy is not enough for test-time adaptation: From the perspective of disentangled factors. In *The Twelfth International Conference on Learning Representations*, 2024.
- [36] Ziwei Liu, Ping Luo, Xiaogang Wang, and Xiaoou Tang. Deep learning face attributes in the wild. In *2015 IEEE International Conference on Computer Vision (ICCV)*, pages 3730–3738, 2015. doi: 10.1109/ICCV.2015.425.
- [37] Barry Becker and Ronny Kohavi. Adult. UCI Machine Learning Repository, 1996.
- [38] Hans Hofmann. Statlog (german credit data). UCI Machine Learning Repository, 1994.
- [39] James Stewart. *Calculus : Early Transcendentals*. Brooks/Cole, Cengage Learning, Belmont, Cal., 2012. ISBN 0-538-49790-4 978-0-538-49790-9 0-8400-5885-3 978-0-8400-5885-0 0-538-49871-4 978-0-538-49871-5 0-538-49887-0 978-0-538-49887-6 0-8400-4825-4 978-0-8400-4825-7.
- [40] Y. Lecun, L. Bottou, Y. Bengio, and P. Haffner. Gradient-based learning applied to document recognition. *Proceedings of the IEEE*, 86(11):2278–2324, 1998. doi: 10.1109/5.726791.
- [41] Alex Krizhevsky. Learning multiple layers of features from tiny images. In *arxiv*, 2009. URL <https://api.semanticscholar.org/CorpusID:18268744>.
- [42] Kaiming He, Xiangyu Zhang, Shaoqing Ren, and Jian Sun. Deep residual learning for image recognition. In *2016 IEEE Conference on Computer Vision and Pattern Recognition (CVPR)*, pages 770–778, 2016. doi: 10.1109/CVPR.2016.90.
- [43] Martin Arjovsky, Léon Bottou, Ishaan Gulrajani, and David Lopez-Paz. Invariant risk minimization, 2020.
- [44] Robert Geirhos, Jörn-Henrik Jacobsen, Claudio Michaelis, Richard Zemel, Wieland Brendel, Matthias Bethge, and Felix A. Wichmann. Shortcut learning in deep neural networks. *Nature Machine Intelligence*, 2(11):665–673, November 2020. ISSN 2522-5839. doi: 10.1038/s42256-020-00257-z.
- [45] Hendrik Heuer, Christof Monz, and Arnold W. M. Smeulders. Generating captions without looking beyond objects, 2016.
- [46] Suchin Gururangan, Swabha Swayamdipta, Omer Levy, Roy Schwartz, Samuel Bowman, and Noah A. Smith. Annotation artifacts in natural language inference data. In Marilyn Walker, Heng Ji, and Amanda Stent, editors, *Proceedings of the 2018 Conference of the North American Chapter of the Association for Computational Linguistics: Human Language Technologies, Volume 2 (Short Papers)*, pages 107–112, New Orleans, Louisiana, June 2018. Association for Computational Linguistics. doi: 10.18653/v1/N18-2017.
- [47] Tom McCoy, Ellie Pavlick, and Tal Linzen. Right for the wrong reasons: Diagnosing syntactic heuristics in natural language inference. In Anna Korhonen, David Traum, and Lluís Màrquez, editors, *Proceedings of the 57th Annual Meeting of the Association for Computational Linguistics*, pages 3428–3448, Florence, Italy, July 2019. Association for Computational Linguistics. doi: 10.18653/v1/P19-1334.
- [48] Shiori Sagawa*, Pang Wei Koh*, Tatsunori B. Hashimoto, and Percy Liang. Distributionally robust neural networks. In *International Conference on Learning Representations*, 2020.

- [49] Zhixuan Chu, Mengxuan Hu, Qing Cui, Longfei Li, and Sheng Li. Task-driven causal feature distillation: Towards trustworthy risk prediction. In *Proceedings of the AAAI Conference on Artificial Intelligence*, volume 38, pages 11642–11650, 2024.
- [50] Ninareh Mehrabi, Fred Morstatter, Nripsuta Saxena, Kristina Lerman, and Aram Galstyan. A survey on bias and fairness in machine learning. *Acm Computing Surveys*, 54(6), July 2021. ISSN 0360-0300. doi: 10.1145/3457607.
- [51] Sara Beery, Yang Liu, Dan Morris, Jim Piavis, Ashish Kapoor, Neel Joshi, Markus Meister, and Pietro Perona. Synthetic examples improve generalization for rare classes. In *Proceedings of the IEEE/CVF Winter Conference on Applications of Computer Vision (WACV)*, March 2020.
- [52] Inwoo Hwang, Sangjun Lee, Yunhyeok Kwak, Seong Joon Oh, Damien Teney, Jin-Hwa Kim, and Byoung-Tak Zhang. SelecMix: Debiased learning by contradicting-pair sampling. In Alice H. Oh, Alekh Agarwal, Danielle Belgrave, and Kyunghyun Cho, editors, *Advances in Neural Information Processing Systems*, 2022.
- [53] Jeonghoon Park, Chaeyeon Chung, Juyoung Lee, and Jaegul Choo. Enhancing intrinsic features for debiasing via investigating class-discerning common attributes in bias-contrastive pair, 2024.
- [54] Hongyi Zhang, Moustapha Cisse, Yann N. Dauphin, and David Lopez-Paz. Mixup: Beyond empirical risk minimization. In *International Conference on Learning Representations*, 2018.
- [55] Taesung Park, Jun-Yan Zhu, Oliver Wang, Jingwan Lu, Eli Shechtman, Alexei A. Efros, and Richard Zhang. Swapping autoencoder for deep image manipulation. In *Proceedings of the 34th International Conference on Neural Information Processing Systems*, Nips '20, Red Hook, NY, USA, 2020. Curran Associates Inc. ISBN 978-1-71382-954-6.

A More visualizations of biased distributions

We plot the biased distributions of more existing benchmarks as follows:

CelebA. CelebA [36] is a dataset for face recognition where each sample is labeled with 40 attributes, which has been adopted as a benchmark for debias methods. Following the experiment configuration suggested by Nam et al. [32], we focus on HeavyMakeup attributes that are spuriously correlated with Gender attributes, i.e., most of the CelebA images with heavy makeup are women. As a result, the biased model suffers from performance degradation when predicting males with heavy makeup and females without heavy makeup. Therefore, we use Heavy_Makeup as the target attribute and Male as a spurious attribute. The joint distribution between the Male and Heavy_Makeup attribute of the CelebA dataset is plotted in Figure 6a. It is clear that the biased distribution of CelebA aligns with that in other existing benchmarks, forming a "diagonal distribution".

WaterBirds. WaterBirds [16] is a synthetic dataset with the task of classify images of birds as "waterbird" and "landbird", which is adopted as a benchmark for debias methods. The label of WaterBirds is spuriously correlated with the image background, i.e. Place attribute, which is either "land" or "water". The joint distribution between the Place and Bird attribute of the WaterBirds dataset is plotted in Figure 6b.

Additional visualization of the biased distribution within real-world datasets is also plotted as follows:

Adult. The Adult [37] dataset, also known as the "Census Income" dataset, is widely used for tasks such as income prediction and fairness analysis. Each sample is labeled with demographic and income-related attributes. The dataset has been adopted as a benchmark for debias methods, particularly focusing on the correlation between race and income. The joint distribution between Race and Income attributes of the Adult dataset is plotted in Figure 6c. It is clear that the biased distribution of Adult does not align with that of other existing benchmarks.

German. The German [38] dataset, also known as the "German Credit" dataset, is commonly used for credit risk analysis and fairness studies. Each sample is labeled with various attributes related to creditworthiness. The dataset serves as a benchmark for debias methods, emphasizing the correlation between age and creditworthiness. The joint distribution between Age and Creditworthiness attributes of the German dataset is plotted in Figure 6d. It is clear that the biased distribution of German does not align with that of other existing benchmarks.

B Fine-grained evaluation framework

In this section, we elaborate on the proposed evaluation framework by mathematically and visually demonstrating the biased distribution within the biased distribution.

Assume a set of biased features $a_i^s \in B$ whose correlated class in the target attribute is defined by a function $g : y^s \rightarrow y^t$, which is an injection from the spurious to the target attribute. The bias magnitude of each biased feature is controlled by $corr_i = P(y^t = g(a_i^s) | y^s = a_i^s)$. Then, the empirical distribution of the biased train distribution satisfies the following equations.

For samples with biased feature a_i^s within B :

$$P(y^s = a_i^s, y^t = a^t) = \begin{cases} P(y^s = a_i^s) * corr_i & \text{if } g(a_i^s) = a^t, \\ \frac{P(y^s = a_i^s) * (1 - corr_i)}{|y^t| - 1} & \text{otherwise,} \end{cases}$$

For samples without biased features and a set of correlated classes $C = \{g(a_i^s) : a_i^s \in B\}$:

$$P(y^s = a^s, y^t = a^t) = \frac{P(y^t = a^t) - \sum_{a_i^s \in B} P(y^s = a_i^s, y^t = a^t)}{|y^s| - |B|}$$

Following the above equations, we further designed LMLP, HMLP, and HMHP biased distributions with the configurations in Table 4. The visualizations of the distributions when the target is a ten-class attribute are in Figure 7.

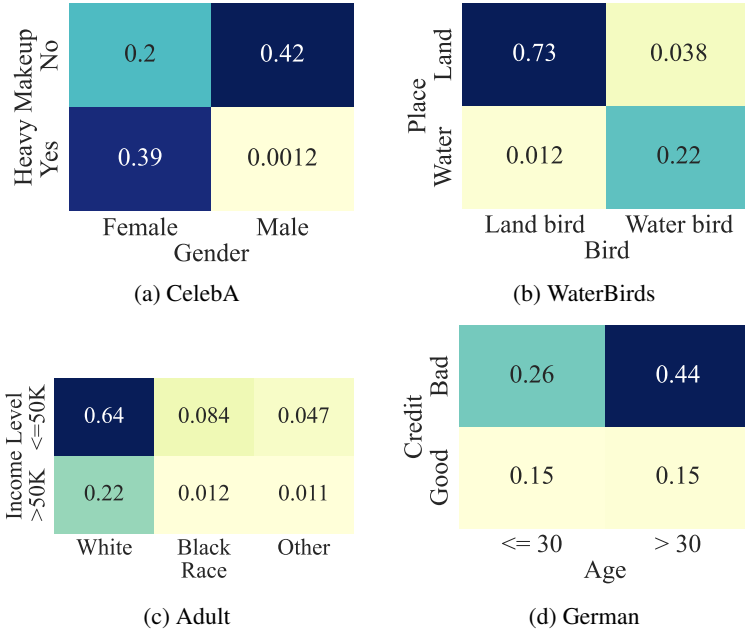


Figure 6: Visualization of the joint distribution for datasets, where the y-axis is the target attribute and the x-axis is the spurious attribute. Figure 6(a) and 6(b) visualize the distribution of existing benchmarks. Figure 6(c) and 6(d) visualize the distribution of real-world datasets. The biased distribution of existing benchmarks and real-world datasets is not alike.

Table 4: Configurations for biased distributions within the proposed evaluation framework

Distribution	$ y^t $	$ B $	$corr_i$
LMLP	10	10	0.5
HMLP	10	1	0.98
HMHP	10	10	0.98
Unbiased	10	0	0.1

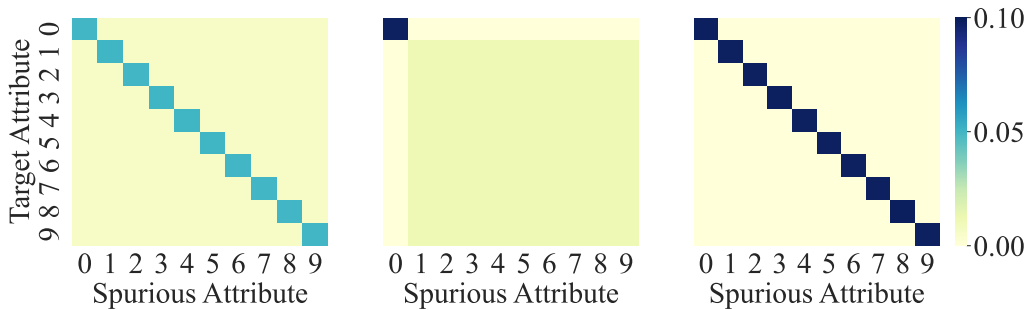


Figure 7: Visualization of biased distributions within the proposed evaluation framework under ten-class classification task. The left, middle, and right plots are visualizations for LMLP, HMLP, and HMHP distribution respectively.

C Theoretical Proofs

C.1 Preliminary

Consider a classification task on binary target attribute $y^t \sim \{-1, +1\}$ and a binary spurious attribute $y^s \sim \{-1, +1\}$. Let the marginal distribution of the target and spurious attribute to be $p_+^t = P(y^t = +1)$ and $p_+^s = P(y^s = +1)$. Then the joint distribution between y^t and y^s can be defined according to the conditional distribution of y^t given $y^s = +1$, i.e. $\tau_+ = P(y^t = +1|y^s = +1)$. Specifically, we can derive the probability of each subgroup in the distribution:

$$P(y^s = +1, y^t = +1) = p_+^s \cdot \tau_+, \quad (5)$$

$$P(y^s = +1, y^t = -1) = p_+^s(1 - \tau_+), \quad (6)$$

$$P(y^s = +1, y^t = -1) = p_+^t - p_+^s \cdot \tau_+, \quad (7)$$

$$P(y^s = -1, y^t = -1) = 1 - p_+^t - p_+^s(1 - \tau_+) \quad (8)$$

We assume that feature $y^s = +1$ and $y^s = -1$ is correlated $y^t = +1$ and $y^t = -1$ respectively, i.e. $\tau_+ > p_+^t$, in the following analysis.

C.2 Proof of proposition 1

Proposition 1 shows that high bias prevalence distribution assumes matched marginal distributions.

Proposition 1. *Assume feature $y^s = +1$ is biased. Then high bias prevalence distribution, i.e. feature $y^s = -1$ is biased as well, implying that the marginal distribution of y^t and y^s is matched, i.e. $p_+^t = p_+^s$. Specifically, as θ approaches to 1, the marginal distribution of y^s approaches to that of y^t , i.e. $\lim_{\theta \rightarrow 1} p_+^s = p_+^t$.*

Proof. We first derive the upper and lower bound of the p_+^s , and then we can prove the proposition with the squeeze theorem [39].

According to the condition that both features in the spurious attribute are biased and the definition of biased feature in ref, we can have the following inequalities:

$$\rho_+ > \theta \cdot \rho_{max}^+ = \theta \cdot (1 - p_+^t), \quad (9)$$

$$\rho_- > \theta \cdot \rho_{max}^- = \theta \cdot p_+^t \quad (10)$$

where $0 < \theta \leq 1$ is the threshold.

We can also derive the simplified bias magnitude of feature $y^s = -1$ based on the conditional distribution, and find its relationship with ρ_+ :

$$\rho_- = \tau_- - p_-^t \quad (11)$$

$$= \frac{1 - p_+^t - p_+^s(1 - \tau_+)}{1 - p_+^s} - (1 - p_+^t) \quad (12)$$

$$= \frac{p_+^s(\tau_+ - p_+^t)}{1 - p_+^s} \quad (13)$$

$$= \frac{p_+^s}{1 - p_+^s} \rho_+ \quad (14)$$

We can then derive the lower bound of p_+^s with the above equation and inequalities:

$$\frac{p_+^s}{1 - p_+^s}(1 - p_+^t) \geq \frac{p_+^s}{1 - p_+^s} \rho_+ = \rho_- \geq \theta \cdot p_+^t \quad (15)$$

$$p_+^s \geq \frac{\theta \cdot p_+^t}{1 - p_+^t + \theta \cdot p_+^t} \geq \theta \cdot p_+^t = LB(\theta) \quad (16)$$

We can also derive the following equation and inequalities of τ_+ according to its definition.

$$\tau_+ = \frac{p_+^s \cdot P(y^s = +1|y^t = +1)}{p_+^s} \leq \frac{p_+^t}{p_+^s} \quad (17)$$

$$\tau_+ = p_+^t + \rho_+ \geq \theta(1 - p_+^t) + p_+^t \quad (18)$$

Then we can derive the upper bound of p_+^s :

$$\theta(1 - p_+^t) + p_+^t \leq \tau_+ \leq \frac{p_+^t}{p_+^s} \quad (19)$$

$$p_+^s \leq \frac{p_+^t}{\theta(1 - p_+^t) + p_+^t} = UB(\theta) \quad (20)$$

We then demonstrate the convergence of the $LB(\theta)$ and $UB(\theta)$ as $\theta \rightarrow 1$:

$$\lim_{\theta \rightarrow 1} LB(\theta) = \lim_{\theta \rightarrow 1} \theta \cdot p_+^t = p_+^t \quad (21)$$

$$\lim_{\theta \rightarrow 1} UB(\theta) = \lim_{\theta \rightarrow 1} \frac{p_+^t}{\theta(1 - p_+^t) + p_+^t} = p_+^t \quad (22)$$

Finally, we can prove the proposition according to the squeeze theorem [39]:

$$LB(\theta) \leq p_+^s \leq UB(\theta) \quad (23)$$

$$\lim_{\theta \rightarrow 1} p_+^s = \lim_{\theta \rightarrow 1} LB(\theta) = \lim_{\theta \rightarrow 1} UB(\theta) = p_+^t \quad (24)$$

C.3 Proof of proposition 2

Proposition 2 shows that high bias prevalence distribution implies uniform marginal distributions.

Proposition 2. *Given that the marginal distribution of y^s and y^t are matched and not uniform, i.e. $p = p_+^s = p_+^t < 0.5$. The bias magnitude of sparse feature, i.e. ρ_+^* , is monotone decreasing at p , with $\lim_{p \rightarrow 0^+} \rho_+^* = -\log(1 - \phi_+)$. The bias magnitude of the dense feature, i.e. ρ_-^* , is monotone increasing at p , with $\lim_{p \rightarrow 0^+} \rho_-^* = 0$.*

Proof. Given the distribution proposed in section C.1 and the condition $p = p_+^s = p_+^t < 0.5$, we further use $\phi_+ = \frac{\rho_+}{\rho_+^{max}}$ to express τ :

$$\tau_+ = p + \phi_+(1 - p) \quad (25)$$

$$\tau_- = 1 - p + \phi_+ \cdot p \quad (26)$$

We can then derive the bias magnitude of the sparse feature $y^s = +1$, given $p = p_+^s = p_+^t < 0.5$, and warp it with a function $t(p)$.

$$\rho_+^* = KL(P(y^t), P(y^t|y^s = +1)) \quad (27)$$

$$= p \cdot \log\left(\frac{p}{\tau_+}\right) + (1 - p) \cdot \log\left(\frac{1 - p}{1 - \tau_+}\right) \quad (28)$$

$$= p \cdot \log\left(\frac{p}{p + \phi_+(1 - p)}\right) + (1 - p) \cdot \log\left(\frac{1 - p}{1 - p - \phi_+(1 - p)}\right) \quad (29)$$

$$= p \cdot \log\left(\frac{p}{p + \phi_+(1 - p)}\right) + (1 - p) \cdot \log\left(\frac{1}{1 - \phi_+}\right) \quad (30)$$

$$= p \cdot \log\left(\frac{p(1 - \phi_+)}{p + \phi_+(1 - p)}\right) + \log\left(\frac{1}{1 - \phi_+}\right) = t(p) \quad (31)$$

We further derive the partial derivative of ρ_+^* on p as follows:

$$\frac{\partial t(p)}{\partial p} = p \cdot \log\left(\frac{p(1 - \phi_+)}{p + \phi_+(1 - p)}\right) + 1 - \frac{p(1 - \phi_+)}{p + \phi_+(1 - p)} \quad (32)$$

Here we apply substitution method to replace $\frac{p(1-\phi_+)}{p+\phi_+(1-p)}$ with x :

$$\frac{\partial t(p)}{\partial p} = f(x) = \log x - (x - 1) \quad (33)$$

$$0 < x = \frac{p(1-\phi_+)}{p+\phi_+(1-p)} \leq 1 \quad (34)$$

We then show that $f(x)$ is monotone increasing in the interval $0 < x \leq 1$ and the critical point is at $x = 1$.

$$f'(x) = \frac{1}{x} - 1 \geq 0 \quad (35)$$

$$f(1) = 0 \quad (36)$$

Thus, we have $f(x) < 0$ in the interval $0 < x \leq 1$, proving $\rho_+^* = t(p)$ to be monotone decreasing at p .

$$\frac{\partial \rho_+^*}{\partial p} = \frac{\partial t(p)}{\partial p} < 0 \quad (37)$$

Similarly, we can derive the bias magnitude of the dense feature $y^s = -1$, and see that it is just $t(1-p)$

$$\rho_-^* = KL(P(y^t), P(y^t|y^s = -1)) \quad (38)$$

$$= (1-p) \cdot \log\left(\frac{(1-p)(1-\phi_+)}{1-p+\phi_+ \cdot p}\right) + \log\left(\frac{1}{1-\phi_+}\right) \quad (39)$$

$$= t(1-p) \quad (40)$$

As a result, we can prove the monotonicity of ρ_-^* with the chain rule.

$$\frac{\partial \rho_-^*}{\partial p} = \frac{\partial t(1-p)}{\partial p} \quad (41)$$

$$= \frac{\partial t(1-p)}{\partial(1-p)} \cdot \frac{\partial(1-p)}{\partial p} \quad (42)$$

$$= -\frac{\partial t(1-p)}{\partial(1-p)} \quad (43)$$

$$= -\frac{\partial t(p)}{\partial p} > 0 \quad (44)$$

We can then derive the convergence of sparse feature bias magnitude ρ_+^* when p approaches 0 with L'Hôpital's Rule [39].

$$\lim_{p \rightarrow 0^+} \rho_+^* = \lim_{p \rightarrow 0^+} t(p) \quad (45)$$

$$= \lim_{p \rightarrow 0^+} \left(p \cdot \log\left(\frac{p(1-\phi_+)}{p+\phi_+(1-p)}\right) \right) + \log\left(\frac{1}{1-\phi_+}\right) \quad (46)$$

$$= \lim_{p \rightarrow 0^+} (p \cdot \log(p)) + \lim_{p \rightarrow 0^+} \left(p \cdot \log\left(\frac{1-\phi_+}{p+\phi_+(1-p)}\right) \right) + \log\left(\frac{1}{1-\phi_+}\right) \quad (47)$$

$$= \lim_{p \rightarrow 0^+} \frac{\log(p)}{\frac{1}{p}} + \log\left(\frac{1}{1-\phi_+}\right) \quad (48)$$

$$= \lim_{p \rightarrow 0^+} \frac{(\log(p))'}{(\frac{1}{p})'} + \log\left(\frac{1}{1-\phi_+}\right) \quad (49)$$

$$= \lim_{p \rightarrow 0^+} \frac{\frac{1}{p}}{-\frac{1}{p^2}} + \log\left(\frac{1}{1-\phi_+}\right) \quad (50)$$

$$= \log\left(\frac{1}{1-\phi_+}\right) \quad (51)$$

Similarly, we can derive the convergence of dense feature bias magnitude ρ_-^* when p approaches to 0.

$$\lim_{p \rightarrow 0^+} \rho_-^* = \lim_{p \rightarrow 0^+} t(1-p) \quad (52)$$

$$= \lim_{p \rightarrow 1^-} (p \cdot \log(\frac{p(1-\phi_+)}{p+\phi_+(1-p)}) + \log(\frac{1}{1-\phi_+})) \quad (53)$$

$$= \log(1-\phi_+) + \log(\frac{1}{1-\phi_+}) \quad (54)$$

$$= 0 \quad (55)$$

D Experiment Details

D.1 Evaluation metrics

Following previous works [9, 12, 15, 17, 18, 20], we use the accuracy of BC samples and the average accuracy on balanced test set as our main metrics. As a complement, we also present the accuracy of BN and BA samples when analyzing the performance of methods. Formally, we categorize samples according to the attributes (y^s, y^t) and a function $g : y^s \rightarrow y^t$ that maps the biased features to its correlated class.

$$BA = \{i | y^s[i] \in B, y^t[i] = g(y^s[i])\} \quad (56)$$

$$BC = \{i | y^s[i] \in B, y^t[i] \neq g(y^s[i])\} \quad (57)$$

$$BN = \{i | y^s[i] \notin B\} \quad (58)$$

where $y^s[i]$ and $y^t[i]$ the attribute value of sample i , and $B = \{a | \rho_a^* > \theta\}$ is the set of biased features.

D.2 Datasets

Colored MNIST [19]. We construct the Colored MNIST dataset based on the MNIST [40] dataset and set the background color as the bias attribute. Different from Colored MNIST used in previous work that simply correlates each of the 10 digits with a distinct color, where the strength of the correlation is controlled by setting the number of bias-aligned samples to $\{0.95\%, 0.98\%, 0.99\%, 0.995\%\}$, we proposed a more fine-grained generation process that is capable of various biased distributions, including LMLP, HMLP, HMHP. See Appendix B for more details.

Corrupted CIFAR10 [12]. We construct the Corrupted CIFAR10 dataset based on the CIFAR10 [41] dataset and set the corruption as the bias attribute. Different from Corrupted CIFAR10 used in previous work that simply correlates each of the 10 objects with a distinct corruption, where the strength of the correlation is controlled by setting the number of bias-aligned samples to $\{0.95\%, 0.98\%, 0.99\%, 0.995\%\}$, we proposed a more fine-grained generation process that is capable of various biased distributions, including LMLP, HMLP, HMHP. See Appendix B for more details.

D.3 Baselines

LfF. Learning from Failure (LfF) [12] is a debiasing technique that addresses the issue of models learning from spurious correlations present in biased datasets. The method involves training two neural networks: one biased network that amplifies the bias by focusing on easily learnable spurious correlations, and one debiased network that emphasizes samples the biased network misclassifies. This dual-training scheme enables the debiased network to focus on more meaningful features that generalize better across various datasets.

DisEnt. The DisEnt [9] method enhances debiasing by using disentangled feature augmentation. It identifies intrinsic and spurious attributes within data and generates new samples by swapping these attributes among the training data. This approach significantly diversifies the training set with bias-conflicting samples, which are crucial for effective debiasing. By training models with these augmented samples, DisEnt achieves better generalization and robustness against biases in various datasets.

BE. BiasEnsemble (BE) [20] is a recent advancement in debiasing techniques that emphasizes the importance of amplifying biases to improve the training of debiased models. BE involves pretraining multiple biased models with different initializations to capture diverse visual attributes associated with biases. By filtering out bias-conflicting samples using these pre-trained models, BE constructs a refined bias-amplified dataset for training the biased network. This method ensures the biased model is highly focused on bias attributes, thereby enhancing the overall debiasing performance of the subsequent debiased model.

D.4 Implementation details

Reproducibility. To ensure the statistical robustness and reproducibility of the result in this work, we repeat each experiment within this work 3 times with consistent random seeds [0, 1, 2]. All results are the average of the three independent runs.

Architecture. Following [9, 12], we use a multi-layer perceptron (MLP) which consists of three hidden layers for Colored MNIST. For the Corrupted CIFAR10 dataset, we train ResNet18 [42] with random initialization.

Training hyper-parameters. We set the learning rate as 0.001, batch size as 256, momentum as 0.9, and number of steps as 25000. We used the default values of hyper-parameters reported in the original papers for the baseline models.

Data augmentation. The image sizes are 28×28 for Colored MNIST and 224×224 for the rest of the datasets. For Colored MNIST, we do not apply additional data augmentation techniques. For Corrupted CIFAR10, we apply random crop and horizontal flip transformations. Also, images are normalized along each channel (3, H, W) with the mean of (0.4914, 0.4822, 0.4465) and standard deviation of (0.2023, 0.1994, 0.2010).

Training device. We conducted all experiments on a workstation with an Intel(R) Xeon(R) Gold 5220R CPU at 2.20GHz, 256 G memory, and 4 NVIDIA GeForce RTX 3090 GPUs. Note that only a single GPU is used for a single task.

D.5 Applying DiD to DBAM methods

As aforementioned in the main paper, when applying our method to the existing DBAM methods [9, 12, 20], we do not modify the training procedure of the debiased model M_d . For both methods, we train the biased model M_b with target feature destroyed data. This is done by simply adding a feature destructive data transformation during data processing, with minimal computational overhead.

Note, for BE [20], such feature destructive data transformation is not applied when training the bias-conflicting detectors.

E Additional Empirical Results

E.1 Detailed results of the main experiments

The main results in the main paper are presented in the form of performance gain and only contain results of BC accuracy and average accuracy on the unbiased test set, here we present the results in their original form, together with error bars, detailed results of accuracies for BA and BN samples of each dataset as well. Results on the Colored MNIST and Corrupted CIFAR10 datasets can be found in Table 5 and Table 6, respectively. It shows that combining DiD not only boosts the performance of existing DBAM methods but also achieves the best performances.

F Related Works

Model Bias. The tendency of machine learning models to learn and predict according to spurious [43] or shortcut [44] features instead of intrinsic features, i.e. model bias, is found in a variety of domains [22, 45, 46, 47, 48] and is of interest from both a scientific and practical perspective. For

Table 5: Results on Colored MNIST dataset show that combining DiD not only boosts the performance of existing DBAM methods but also achieves the best performances. The accuracy of BN samples is marked as '-' in LMLP and HMHP distribution for there is no BN sample within the dataset according to our evaluation setting in Appendix D.

Distr.	Algorithm	Accuracy			
		BA acc	BC acc	BN acc	Avg acc
LMLP	ERM	97.73 \pm 0.09	91.13 \pm 0.17	-	91.73 \pm 0.16
	LfF	80.25 \pm 4.86	68.41 \pm 2.01	-	69.74 \pm 2.41
	+ DiD	92.16 \pm 0.35	91.03 \pm 0.15	-	91.15 \pm 0.17
	LfF BE	82.95 \pm 1.68	83.60 \pm 0.85	-	83.53 \pm 0.75
	+ DiD	93.49 \pm 0.81	89.25 \pm 0.64	-	89.67 \pm 0.54
	DisEnt	84.45 \pm 1.72	73.87 \pm 2.52	-	74.93 \pm 2.44
	+ DiD	94.03 \pm 0.66	91.09 \pm 0.24	-	91.38 \pm 0.28
	DisEnt BE	80.18 \pm 1.94	81.07 \pm 2.50	-	80.98 \pm 2.29
	+ DiD	91.89 \pm 0.26	89.80 \pm 0.97	-	90.01 \pm 0.89
	HMLP	ERM	99.32 \pm 0.34	85.25 \pm 1.62	90.30 \pm 0.56
LfF		87.76 \pm 4.12	57.98 \pm 3.58	63.72 \pm 3.22	63.35 \pm 3.02
+ DiD		82.99 \pm 5.08	90.54 \pm 0.74	89.04 \pm 0.84	89.12 \pm 0.77
LfF BE		57.65 \pm 32.14	80.02 \pm 1.10	82.84 \pm 1.68	82.33 \pm 1.93
+ DiD		63.95 \pm 15.64	89.11 \pm 1.29	87.28 \pm 1.54	87.22 \pm 1.58
DisEnt		77.55 \pm 7.93	66.52 \pm 8.75	72.69 \pm 5.91	72.18 \pm 6.05
+ DiD		88.78 \pm 7.24	88.52 \pm 1.47	89.04 \pm 1.13	88.99 \pm 1.16
DisEnt BE		41.84 \pm 6.21	77.59 \pm 0.69	80.87 \pm 1.78	80.19 \pm 1.71
+ DiD		31.97 \pm 7.08	89.33 \pm 1.07	85.88 \pm 0.86	85.66 \pm 0.89
HMHP		ERM	99.57 \pm 0.07	48.54 \pm 1.22	-
	LfF	57.16 \pm 8.27	65.62 \pm 2.87	-	64.59 \pm 3.31
	+ DiD	77.84 \pm 2.49	66.91 \pm 1.73	-	68.00 \pm 1.80
	LfF BE	73.61 \pm 1.03	66.90 \pm 0.43	-	67.57 \pm 0.47
	+ DiD	85.65 \pm 2.53	66.37 \pm 2.54	-	68.30 \pm 2.50
	DisEnt	59.89 \pm 4.19	68.29 \pm 1.43	-	67.45 \pm 1.28
	+ DiD	83.65 \pm 0.13	69.05 \pm 0.38	-	70.51 \pm 0.33
	DisEnt BE	77.74 \pm 2.51	67.51 \pm 1.33	-	68.53 \pm 1.45
	+ DiD	84.62 \pm 1.16	69.50 \pm 1.23	-	71.01 \pm 1.08

example, visual recognition models may overly rely on the background of the picture rather than the targeted foreground object during prediction. One subtopic of model bias is model fairness, which generally refers to the issue that social biases are captured by models [25], where the spurious features are usually human-related and annotated, such as gender, race, and age [23, 38, 38].

Data Bias: spurious correlation. Generally, spurious correlation refers to the phenomenon that two distinct concepts are statistically correlated within the training distribution, though there is no causal relationship between them, e.g. background and foreground object [49]. The spurious correlation is a vital aspect of understanding how machine learning models learn and generalize [43]. Specifically, studies on distribution shift [6] claim that spurious correlation is one of the major types of distribution shift in the real world, and thus an important distribution shift that a reliable model should be robust to. Furthermore, studies on fairness and bias [50] have demonstrated the pernicious impact of spurious correlation in classification [34], conversation [51], and image captioning [22]. However, despite its broad impact, spurious correlation is generally used as a vague concept in previous works and lacks a proper definition and deeper understanding of it. This is also the major motivation of this work.

Table 6: Results on Corrupted CIFAR10 dataset show that combining DiD not only boosts the performance of existing DBAM methods but also achieves the best performances. The accuracy of BN samples is marked as ‘-’ in LMLP and HMHP distribution for there is no BN sample within the dataset according to our evaluation setting in Appendix D.

Distr.	Algorithm	Accuracy			
		BA acc	BC acc	BN acc	Avg acc
LMLP	ERM	80.40 \pm 0.81	62.50 \pm 0.15	-	64.29 \pm 0.06
	LfF	59.13 \pm 0.68	55.03 \pm 0.04	-	55.44 \pm 0.09
	+ DiD	69.47 \pm 0.96	62.04 \pm 0.21	-	62.78 \pm 0.10
	LfF BE	70.87 \pm 1.30	52.10 \pm 0.30	-	53.98 \pm 0.40
	+ DiD	63.23 \pm 2.10	53.21 \pm 0.20	-	54.21 \pm 0.38
	DisEnt	61.58 \pm 0.57	55.45 \pm 0.23	-	56.06 \pm 0.17
	+ DiD	72.23 \pm 0.74	60.84 \pm 0.40	-	61.98 \pm 0.30
	DisEnt BE	62.73 \pm 0.61	56.59 \pm 0.08	-	57.20 \pm 0.13
	+ DiD	65.98 \pm 0.40	60.92 \pm 0.20	-	61.42 \pm 0.21
	HMLP	ERM	84.67 \pm 0.64	55.85 \pm 0.17	65.75 \pm 0.00
LfF		73.33 \pm 1.67	47.70 \pm 0.58	54.58 \pm 0.49	54.15 \pm 0.41
+ DiD		78.67 \pm 2.14	54.81 \pm 2.26	63.71 \pm 2.69	63.06 \pm 2.63
LfF BE		70.33 \pm 2.19	50.96 \pm 2.35	54.14 \pm 0.25	54.02 \pm 0.36
+ DiD		68.80 \pm 0.88	50.20 \pm 0.79	54.39 \pm 0.18	54.15 \pm 0.15
DisEnt		61.67 \pm 1.67	52.48 \pm 0.56	54.65 \pm 0.56	54.53 \pm 0.49
+ DiD		73.67 \pm 2.64	55.26 \pm 0.93	62.11 \pm 0.17	61.61 \pm 0.13
DisEnt BE		75.33 \pm 5.21	49.15 \pm 1.54	56.86 \pm 0.30	56.35 \pm 0.35
+ DiD		78.40 \pm 1.00	54.09 \pm 1.07	62.05 \pm 0.34	61.50 \pm 0.38
HMHP		ERM	89.97 \pm 0.34	29.37 \pm 0.30	-
	LfF	72.70 \pm 0.81	35.30 \pm 0.33	-	39.04 \pm 0.33
	+ DiD	82.07 \pm 1.09	37.05 \pm 0.31	-	41.55 \pm 0.19
	LfF BE	82.73 \pm 0.92	31.48 \pm 0.82	-	36.61 \pm 0.65
	+ DiD	78.30 \pm 0.47	32.90 \pm 1.79	-	37.44 \pm 1.61
	DisEnt	70.77 \pm 2.27	36.04 \pm 0.62	-	39.51 \pm 0.36
	+ DiD	76.60 \pm 0.70	39.05 \pm 0.35	-	42.80 \pm 0.25
	DisEnt BE	78.60 \pm 1.56	34.20 \pm 0.43	-	38.64 \pm 0.38
	+ DiD	78.70 \pm 1.47	37.72 \pm 0.96	-	41.82 \pm 0.91

Spurious correlation debiasing. In this work, we focus only on debias methods that do not require bias information, i.e. without annotation on the spurious attribute, for it is more practical. The mainstream of work [9, 12, 15, 17, 18, 20, 52, 53] in the area of spurious correlation debiasing follows the framework proposed by Nam et al. [12], which introduces a biased auxiliary model to capture biases within the training data, according to which a re-weighting scheme designed to emphasize BC samples is applied to train a debiased model, i.e. *DBAM methods*. Based on the framework, Lee et al. [9] further proposed a feature augmentation technique to further enhance BC samples. Hwang et al. [52] proposed to augment biased data by applying mixup [54] to contradicting pairs. Lim et al. [17] proposed an adversarial-based approach to augment BC samples aiming to increase the diversity of BC samples. Lee et al. [20] proposed to first filter out BC samples before training the biased model aiming to enhance the bias capture process of the biased model. Liu et al. [16] regard the samples misclassified by the model trained with empirical risk minimization as BC samples and emphasize them during training of a debiased model. Recently, Park et al. [53] proposed to provide models with explicit spatial guidance that indicates the region of intrinsic features.

Among other lines of work, Park et al. [53] create images without bias attributes using an image-to-image translation model [55]. A recent pair-wise debiasing method χ^2 model [9] encourages the model to retain intra-class compactness using samples generated via feature-level interpolation between BC and BA samples.

G Limitations and Future Work

We uncover the insufficiency of existing debiasing benchmarks theoretically and empirically, highlighting the importance of debiasing on real-world biases. We further proposed a feature-destruction-based method that focuses on DBAM methods. However, there are still a few limitations of this work:

- While DBAM methods are the predominant works in debiasing, there are also other lines of work such as data generation methods. Thus, one limitation is that We have not evaluated such methods with our proposed evaluation framework which might also yield some interesting insights on debiasing.
- Another limitation is that, though we have already seen the potential of target feature destruction, whether it can be applied to other lines of work remains to be studied.
- As shown in section E, while our proposed approach effectively improves the performance of existing DBAM methods on all biased distributions from the real world, the performance is still far from satisfactory, which remains to be further improved in future works.

We see potential within those limitations and leave them for future research.

H Boarder Impact

From a technical standpoint, our research provides a comprehensive framework for analyzing and mitigating biases in datasets. The proposed fine-grained analysis framework and evaluation benchmarks offer a new perspective on how biases manifest in real-world data and how existing debias methods can be improved. Our approach, which involves the destruction of target features during bias capture, demonstrates significant improvements in handling real-world biases, as evidenced by our extensive experimental results.

By advancing the understanding of dataset biases and improving the performance of debias methods, our research contributes to the development of more robust and generalizable AI models. This is particularly relevant in an era where AI systems are increasingly deployed in dynamic and diverse environments, necessitating models that can adapt and maintain high performance across different contexts and populations.